

ACCEPTED MANUSCRIPT

On diagnostics of an annular shape RF plasma jet operating in Ar at atmospheric conditions

To cite this article before publication: Ivana Sremaki *et al* 2020 *Plasma Sources Sci. Technol.* in press <https://doi.org/10.1088/1361-6595/ab71f7>

Manuscript version: Accepted Manuscript

Accepted Manuscript is “the version of the article accepted for publication including all changes made as a result of the peer review process, and which may also include the addition to the article by IOP Publishing of a header, an article ID, a cover sheet and/or an ‘Accepted Manuscript’ watermark, but excluding any other editing, typesetting or other changes made by IOP Publishing and/or its licensors”

This Accepted Manuscript is © 2020 IOP Publishing Ltd.

During the embargo period (the 12 month period from the publication of the Version of Record of this article), the Accepted Manuscript is fully protected by copyright and cannot be reused or reposted elsewhere.

As the Version of Record of this article is going to be / has been published on a subscription basis, this Accepted Manuscript is available for reuse under a CC BY-NC-ND 3.0 licence after the 12 month embargo period.

After the embargo period, everyone is permitted to use copy and redistribute this article for non-commercial purposes only, provided that they adhere to all the terms of the licence <https://creativecommons.org/licenses/by-nc-nd/3.0>

Although reasonable endeavours have been taken to obtain all necessary permissions from third parties to include their copyrighted content within this article, their full citation and copyright line may not be present in this Accepted Manuscript version. Before using any content from this article, please refer to the Version of Record on IOPscience once published for full citation and copyright details, as permissions will likely be required. All third party content is fully copyright protected, unless specifically stated otherwise in the figure caption in the Version of Record.

View the [article online](#) for updates and enhancements.

On diagnostics of an annular shape RF plasma jet operating in Ar at atmospheric conditions

Ivana Sremački^{a,*}, Andrea Jurov^b, Martina Modic^b, Uroš Cvelbar^b, Lei Wang^a, Christophe Leys^a, Anton Nikiforov^a

^a*Department of Applied Physics, Ghent University, Sint-Pietersnieuwstraat 41, Gent, 9000, Belgium, EU*

^b*Jozef Stefan Institute, Jamova cesta 39, Ljubljana, 1000, Slovenia, EU*

E-mail: ivana.sremacki@ugent.be

Abstract

One of the driving forces behind the development of cold plasma sources at atmospheric pressure is an application in the biomedical field. In this respect, the radio-frequency (RF) plasma jets are of particular importance due to possible safe operation on humans and a generation of the high amount of reactive species. For this reason, we designed RF plasma jet in co-axial geometry with the possibility of aerosol introduction, where its characteristics were evaluated by electrical diagnostics, optical emission, and laser scattering spectroscopy. The RF plasma jet operation and stability of diffuse mode were analysed based on energy balance. It was observed that α mode diffuse discharge characterized by effluent length up to 5 mm was sustained at power density below 30 W/cm^3 . The gas and rotational temperature were determined by means of spectroscopy methods and compared with results of direct laser scattering. It was established that gas temperature obtained from N_2 emission of transition $\text{C}^3\Pi_u \rightarrow \text{B}^3\Pi_g (0,2)$ is highly overestimated whereas the gas temperature estimated from OH transition $\text{A}^2\Sigma^+ \rightarrow \text{X}^2\Pi_1 (0,0)$ gave a reasonable agreement with both Rayleigh and Raman spectroscopy. Based on Rayleigh scattering method uniform gas temperature distribution in the discharge effluent was found at power below 15 W with average temperature below $340 \pm 15 \text{ K}$. The low gas temperature of Ar plasma jet allows using this source in temperature sensitive material applications including skin treatments.

Keywords: RF plasma jet, cold plasma, plasma diagnostics, laser scattering, Rayleigh spectroscopy, Raman spectroscopy

1. Introduction

Low-temperature atmospheric pressure plasmas are a powerful source of chemically active species that are used for different heat-sensitive material processing or even in gas cleaning and synthesis and chemical synthesis, materials surface functionalisation, cleaning, etching, coating, etc [1, 2]. Interest in these plasmas as a tool increased over the years due to various applications in plasma medicine. Their capabilities to generate reactive oxygen and nitrogen species (ROS, RNS), enabled them to be used for the inactivation of microorganisms, stimulate cell proliferation, tissue regeneration or even inactivate cells by initializing apoptosis [3]. During the last years, two basic plasma device principles were established in medical research and application [4-6], known as dielectric barrier discharge (DBD) and atmospheric pressure plasma jet (APPJ). The safe application of plasma requires the generation of stable and reproducible plasma which is capable to operate at atmospheric conditions. Furthermore, plasma needs to be cold (under temperatures that could induce skin burnings) and electromagnetic compatible (there should be no EM coupling between source and substrate) [3]. Here, APPJs are especially interesting due to plasma effluent created in surrounding air suitable for direct treating of substrates [7, 8]. The fact that plasma is in direct contact with air makes plasma physics and chemistry of atmospheric pressure jets rather complex and brings a number of complications into its evaluations with plasma diagnostics.

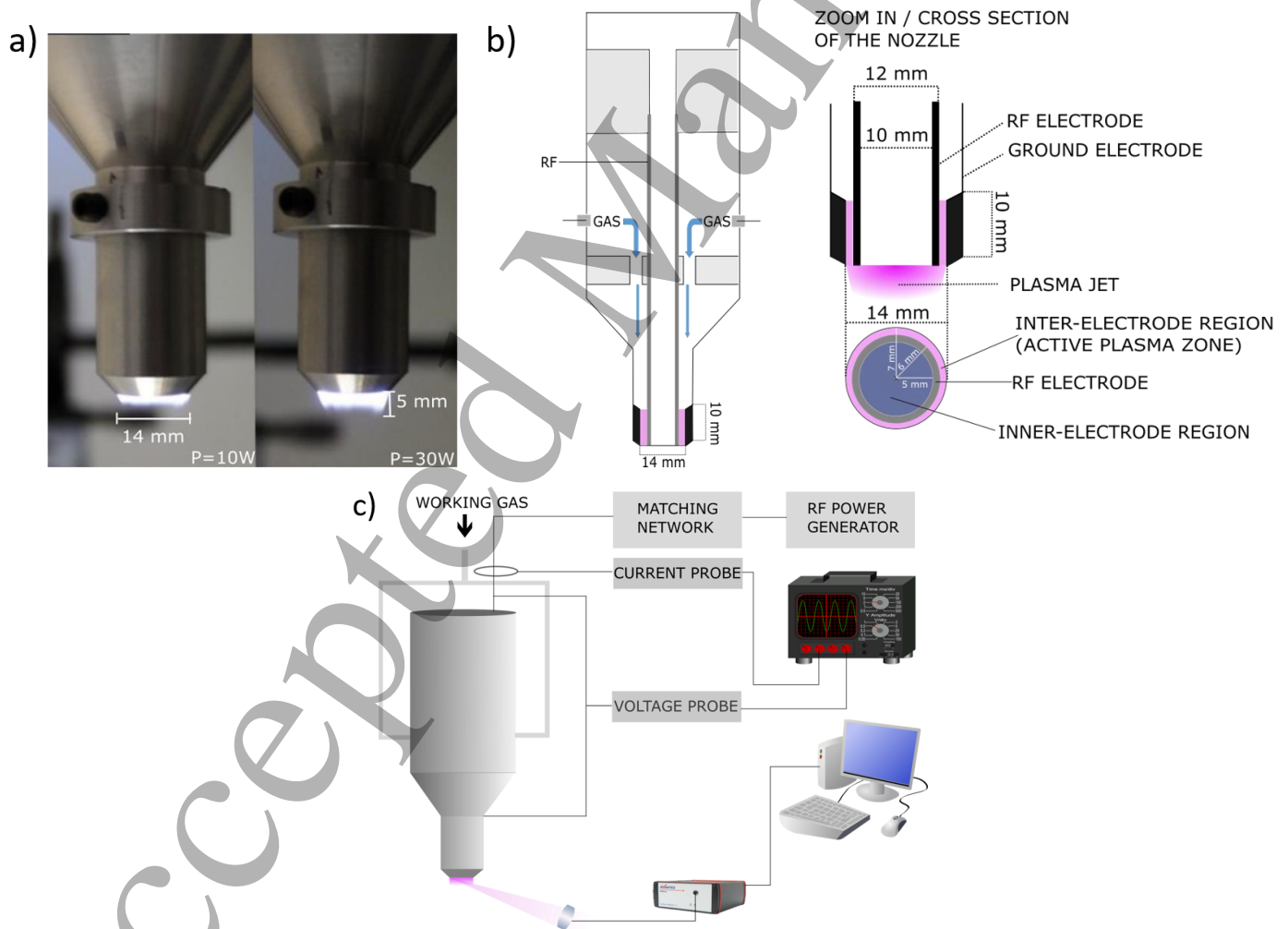
To design a source that meets previous requirements, a set of experimental plasma diagnostics is needed. For this reason, the present work was focused on electrical and temperature characterization of argon atmospheric pressure radio-frequency plasma jet. Plasma source is designed in so-called co-axial electrode geometry, first introduced by Selwyn et al. [9] and Döbele et al [10]. In contrast to aforementioned works where discharge in He was studied, an attempt is made in current study to generate stable plasma in Ar gas. It has to be noted that for industrial and medical applications, cold plasmas in argon have advantage over expensive He gas. However, design of the reactor should enable safe and stable operation which is often not a case for APPJs operating in Ar because of filaments formation [11]. The source developed here is based on works [9, 12, 13] and it is an RF plasma up-scaled in form of ring-shaped jet of 14 mm diameter operating in pure Ar under atmospheric conditions. The source is intended to be used for skin treatment to support safe and fast wound healing and plasma/aerosol assisted topical drug introduction. Accordingly, it is constructed in a way that simultaneous application of water-soluble pharmaceutical compounds and plasma is possible. Hereby, the aim of this work is to study the source operating in Ar and suitable for combination with an aerosol, to investigate its electrical characteristics and compare temperature diagnostic methods applied to accurately measure gas temperature (T_g) in the plasma effluent. The most convenient way to measure gas temperature in non-equilibrium plasmas is rotational optical emission spectroscopy (OES) of molecules. Temperature diagnostics by optical emission spectroscopy is well examined for rotational lines of the same vibrational band for N_2 transition $C^3\Pi_u \rightarrow B^3\Pi_g$ (0,2) and OH transition $A^2\Sigma^+ \rightarrow X^2\Pi_i$ (0,0) [14, 15]. This technique is based on the fact that plasma has to fulfil rotational-translational equilibrium described by the Maxwell-Boltzmann distribution of populated rotational levels. However in atmospheric pressure plasmas, due to quenching effects and ro-vibrational coupling of states, overpopulation of higher rotational levels has been noticed in many cases. This overpopulation is manifested as non-Boltzmann behaviour resulting in overestimation T_g [16]. The complexity of optical emission spectra analysis for gas temperature determination is coupled with a low spatial resolution of the method due to the line of sight detection. This is also a method disadvantage and its validity needs to be improved by other techniques such as laser radiation scattering. Better spatial resolution and higher sensitivity are obtained by the Rayleigh scattering with a scattered signal intensity directly proportional to heavy particle density. The method of laser scattering has been applied to measure gas temperature in high-pressure arc [17] and recently to APPJs [18]. The approximation of the negligible effect of plasma on the gas flow is not always valid. In many cases, the gas flow is strongly affected by plasma and even is controlled by the discharge as done e.g. in plasma actuators [19, 20]. To confirm that the effect of plasma on gas dynamics in our RF discharge is negligible, the Rayleigh temperature measurements are confirmed by Raman scattering spectroscopy. The advantage of Raman scattering technique is based on inelastic scattering of laser light on molecules in ground states and is independent of gas-phase dynamics [21]. Armed with this data, we were able precisely to determine the set of operational conditions at which the RF jet is safe for treatment of skin, and at the same time re-validate spectroscopy methods capability for gas temperature measurements at conditions of RF APPJ propagating in ambient air.

2. Materials and methods

In the presented paper, RF plasma jet for treatment large size objects and compatible with direct injection of an aerosol is studied. The main focus is given on the analysis of the RF plasma jet electrical characteristics and operational window for stable operation in diffuse α mode. The gas temperature T_g as a key parameter for biomedical applications is studied by a combination of different methods. Chosen methods are applied in a way that they cannot affect the properties of the plasma. They are considered noninvasive, whereas T_g in the plasma afterglow is determined by three different spectroscopic techniques; optical emission spectroscopy (OES), Rayleigh and Raman scattering spectroscopy. The application of methods is based on the analysis of different physical processes, which allows comparison and validation of diagnostic methods in the high-pressure non-equilibrium discharges.

2.1 RF plasma jet source and its electrical characterisation

1 The plasma source presented in Figure 1 was consisted of two coaxial electrodes with an internal one made as a hollow cylinder of
 2 $d_{in}= 10$ mm and $d_{out}= 12$ mm. The internal electrode from stainless steel, powered by RF voltage, was surrounded by grounded
 3 external electrode of 14 mm diameter. The grounded outer electrode was made of aluminium. As can be seen from Figure 1 the
 4 conical reductions were made in the source body for practical reasons of the source installation and it's holding. Additionally conical
 5 reduction in lowest part of the source was made of a size that fits in standard 12-well plate for bio-tests. The plasma source was
 6 powered with RF generator CESAR 136 (Advanced Energy Industries) operating at 13.56 MHz with L-type matching box. The
 7 inter-electrode gap of 1 mm width and 10 mm length was formed by reduction of the grounded electrode diameter from 20 mm to
 8 14 mm as shown in Figure 1(b). The gas was fed into the gap through two inlets mounted symmetrically 10 cm above the electrodes
 9 that insure a laminar flow of the gas at the outlet of the source. For purposes of plasma diagnostics N_2 (99.999% purity) or dry air
 10 (78.999% N_2 and 21% O_2) were added to gas mixture in an amount of 0.05-0.2% of argon flow. This very small amount of admixing
 11 gas insured that effect of admixing gas was negligible on electrical and temperature properties of the discharge. Depending on the
 12 jet application argon flow was chose of 2 slm (standard liter per minute), 3, and 4 slm which corresponds to Reynolds numbers
 13 120, 180 and 240 indicating the laminar gas flow. In case of gas flow higher than 4 slm, the discharge cannot be sustained in stable
 14 mode. Electric current and voltage of the discharge were measured with IV probe (Vigilant) and were recorded with an oscilloscope
 15 (LeCroy Wavesurfer). Fast imaging with 5 ns resolution in single-shot mode was performed with the use of Hamamatsu ICCD
 16 camera with a bandpass filter with a transparency of 10 nm full width at half maxima (FWHM) centered at 750 nm. The camera
 17 was placed in front of the plasma jet and focused on the edge of the nozzle. ICCD camera was synchronised with RF generator with
 18 use of a delay generator Stanford Research DG535. The visual image of the plasma effluent, cross-section of the reactor and the
 19 nozzle with indicated regions of interest and experimental setup for electrical and optical characterisation of the plasma jet are
 20 presented in Figure 1(a,b).



59 **Figure 1.** a) Visual view of the jet effluent in ambient air indicating the effluent formation of a length of 5 mm for the highest RF
 60 power applied at Ar flow of 2 slm; b) Cross-section of the reactor, enlarged nozzle and its cross-section with indicated regions of interest c) Experimental set-up schematics used for optical and electrical characterisation of RF plasma jet.

2.2 Optical emission spectroscopy

APPJs are non-equilibrium plasmas with present constituents that have different temperatures (electronic T_e , vibrational T_{vib} , translational T_t and rotational temperature T_{rot}). In case of non-equilibrium atmospheric plasmas, the rotational temperature can be used as an indicator of the gas translational temperature due to the very high frequency of the collisions leading to establishing of the equilibrium between different rotational states of the colliders. Indeed as the lifetime of the molecules in the excited states is normally significantly larger than the characteristic time between collisions, the rotational temperature of the excited state is usually a good representation of the gas temperature [14, 16]. Accordingly, the establishing of the gas temperature in APPJ involves the determination of T_{rot} of present molecules. The most atmospheric pressure plasma diagnostics are based on the use of emission from OH(A) states or N_2 as an indicator of T_{rot} , considering their presence in many atmospheric pressure plasmas. OES temperature measurements are based on relative intensity measurements of rotational lines in the same vibrational band. Following Boltzmann distribution of rotational states, it is possible to directly infer translation temperature from rotational temperature. Here, the measurements of the gas temperature were done from partially rotationally resolved emission from OH radicals transition $A^2\Sigma^+ \rightarrow X^2\Pi_i(0,0)$ with a maximum of emission around 309 nm [14, 22] as well as from $N_2 C^3\Pi_u \rightarrow B^3\Pi_g(0,2)$ band with a maximum at 380 nm. Molecule rotational spectra were recorded using Avantes spectrometer with a resolution of 0.05 nm with optical fibre directed to the effluent where plasma properties have been measured. Considering axial symmetry of the plasma source it is expected that plasma radiation is collected from the region corresponding to the inter-electrode area, e.g. for an area at 6 to 7 mm across of the jet as shown on Figure 1(b).

OES is an experimentally simple, none invasive, none expensive as well as a fast method for estimation of the plasma parameters. Despite its simplicity, the method provides a line of sight measurement of the T_g and relies on the approximation that T_g is equivalent to T_{rot} of the excited states. Such an approach can lead to pitfalls and drastic overestimation of the gas temperature [16]. Typically the use of OH (A) emission leads to an overestimation of gas temperature due to non-Boltzmann behaviour of the rotational states with high J numbers ($J > 12$) [15, 22]. However, the use of N_2 emission can also result in incorrect estimates of the gas temperature, especially in the case of discharges operating in Ar gas [23]. Since this work is focused on accurate temperature measurements of the plasma jet, two direct methods of plasma diagnostics by laser scattering were applied to validate results of OES. Laser-based spectroscopy methods, namely Rayleigh and Raman scattering spectroscopy, overcome disadvantages of the OES method. Both methods are well spatially resolved, based on elastic laser scattering on heavy particles (Rayleigh) or inelastic laser scattering (Raman) and capable of direct measurements of translation temperature of ground states.

2.3 Rayleigh scattering laser spectroscopy

Rayleigh scattering spectroscopy is an active spectroscopic method based on the elastic scattering of laser light on heavy particles. A detailed description of the Rayleigh scattering theory is found in [24, 25]. The intensity of the scattered light depends on the intensity and polarisation of the incident light, and the density of the scatterers n_g^i .

$$I \sim \sum_i \sigma^i n_g^i = \sum_i \sigma^i \frac{p^i}{k_B T_g}, \quad (1)$$

where σ^i is the Rayleigh scattering cross-section of the light on i scatterer and p^i is a partial pressure of the scatterer in the gas mixture. The direct dependence of the scattering signal on the density of heavy particles allows using the method for spatial and temporal resolved gas temperature measurements. For plasma temperature measurements, two signals in the same conditions need to be recorded: reference signal I_0 in working gas without plasma at referent temperature T_0 , and the signal from the plasma I_p with unknown T_g . Accordingly, the temperature T_g is calculated as:

$$T_g = \frac{I_0}{I_p} T_0. \quad (2)$$

Recorded scattered signal is a signal originating from different heavy particles present in the discharge. In argon plasma operating in ambient air following species are considered: Ar, N_2 , and O_2 . Since these species have a similar cross-section for Rayleigh scattering, the signal can be considered independent of the mixture and air entrainment in the effluent [26].

For temperature measurements pulsed Nd:YAG laser (Litron nano-S) was used at a wavelength of 532 nm. The repetition rate was 10 Hz, energy of the pulse was set to 8 mJ and pulse duration was 8 ns. Laser beam had a Gaussian shape with a diameter of 8 mm. At 532 nm light scattered cross-sections on Ar atoms and air are $4.5 \cdot 10^{-27}$ and $5.245 \cdot 10^{-27}$ respectively in units $cm^2/molecule$ [25]. Fast imaging gated Hamamatsu digital camera with 532 nm filter with FWHM of 10 nm was used to record a scattered signal from the region of interest when plasma was OFF and ON in order to measure the signal I_0 and I_p , respectively. The synchronisation between the laser pulse and the camera gate unit was achieved using Stanford Research DG535 delay generator. Experimental set up for Rayleigh scattering spectroscopy is shown in Figure 2(a).

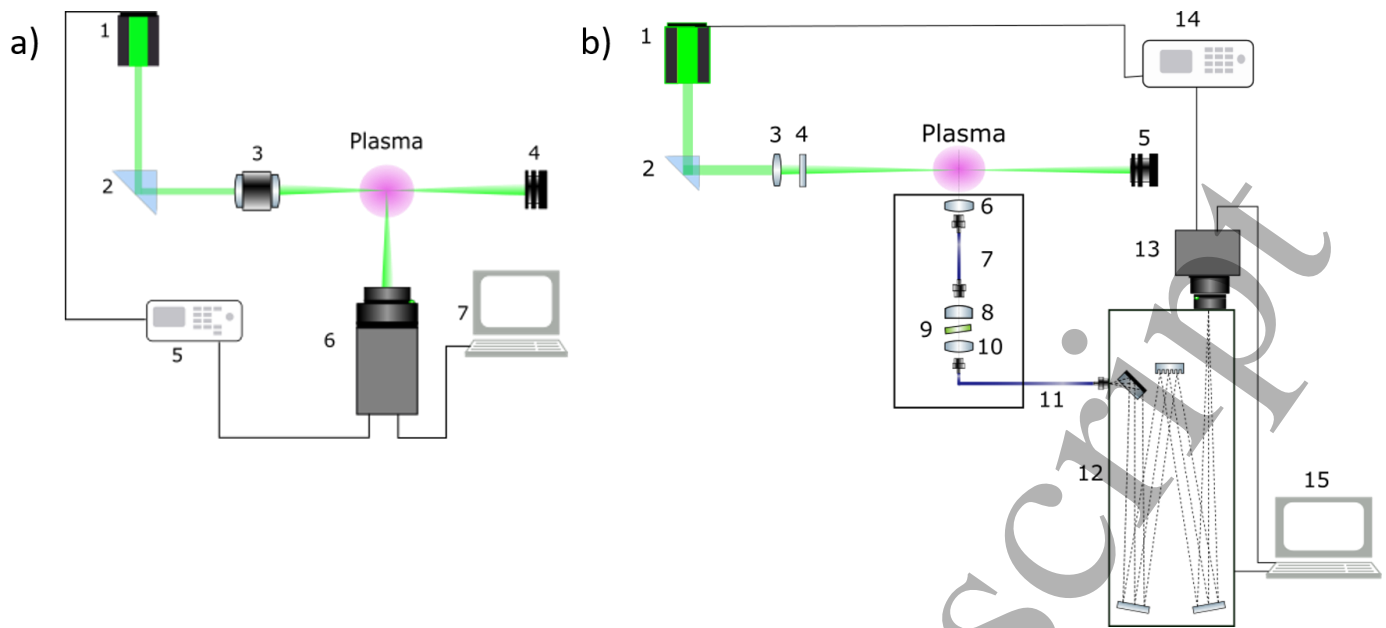


Figure 2. Experimental schematic of setup for: **a)** Rayleigh scattering spectroscopy with 1-Nd:YAG laser at 532 nm, 2-90 degree rotation prism, 3-telescope, 4-beam dump, 5-delay generator, 6-camera, and 7-PC; **b)** Raman scattering spectroscopy with 1-Nd:YAG laser at 532 nm; 2-prism; 3-lens $f=500$ mm; 4-polarizer; 5-beam dump; 6,10 - collecting lens $f=50$ mm; 7,11 - optical fiber with diameter of $300 \mu\text{m}$; 8- collimation lens $f=30$ mm; 9- BNF 532 nm; 12-Monochromator; 13- ICCD camera; 14-delay generator; and 15-PC.

Quartz prism was used to deflect the direction of beam propagation for 90° . After deflection, the beam was reduced using the Edmund Optics telescope of power 10X, so the beam diameter in the plasma region was 0.8 mm. Temperature measurements were done at a distance 1.5 mm from the nozzle in the effluent with spatial resolution along the jet better than $50 \mu\text{m}$. The rationality in choice of the distance is dictated by biomedical applications of the developed source as typically treated objects are located at 1.5 mm from the nozzle. Experiments were carried out in ambient air. Only the region of interest, defined later on in the paper, was used for Rayleigh scattering analysis. In order to perform a proper comparison of the Rayleigh scattering results with space averaged results of the OES the Rayleigh signal was averaged over 1 mm region corresponding to the inter-electrode region of elevated temperature. It has to be emphasized that eq. (1) and (2) are applicable only in a case when the electrical discharge operation is not affecting the gas flow dynamics. Otherwise observed Rayleigh signal during plasma operation has to be attributed not only to change of the T_g but also to change of p^i in eq. (2) which appears due to plasma effect on the gas flow. To this end applicability of the Rayleigh scattering method applied for T_g measurements was furthermore validated by the Raman laser scattering. Since RF APPJ is designed to be used for medical treatment all experiments were carried out in conditions as close to real situation as possible without any shielding gas. As it is known the Mie scattering can strongly affect both Rayleigh and Raman measurements. In order to suppress the Mie scattering effect only an area underneath of the nozzle free of Mie scattering was analysed in laser scattering tests.

2.4 Raman laser scattering spectroscopy

Raman scattering spectroscopy is based on inelastic scattering of laser light on molecules, and for this purpose, dry air was added at 0.2 v.% to the feed gas. A spectrum consists of two symmetrical wings called Stokes and Anti-Stokes components with lines shifted relative to central incident wavelength (λ_L). The challenging task of the rotational Raman spectroscopy is very low scattering signal intensity and partial overlap of the central lines with about 10^4 times higher Rayleigh signal that requires filtration of the elastically scattered light out in order to avoid saturation of the detector. Details of the Raman scattering spectroscopy are found in the literature [21, 27-29]. Since Raman rotational spectra is a characteristic of a specific molecule, the spectra are species dependent, and so the method is free of the disadvantage of Rayleigh scattering spectroscopy. Wavelengths of Anti-Stokes and Stokes component for transitions J - J' are calculated using the expression [30]:

$$\lambda_{J-J'} = \lambda_L + \frac{\lambda_L^2}{hc} B_v ((J'^2 + J') - (J^2 + J)), \quad (3)$$

here h and c are Planck constant and the speed of the light respectively, B_v rotational constant of molecules N_2 and O_2 , J and J' are quantum numbers of initial and final rotational state. The light intensity of Raman transition J - J' is calculated as [31]:

$$I_{J-J'} = C n_J \frac{d\sigma_{J-J'}}{d\Omega}, \quad (4)$$

where C is the experimental constant, n_J is a density of molecules in states J and $d\sigma_{J-J'}/d\Omega$ is a differential cross-section for transition $J-J'$. The density of molecules in state J is given as [32]:

$$n_J = \frac{n}{Q} (2J + 1) g_J e^{-\frac{B_v J(J+1)}{kT}}, \quad (5)$$

where n is a density of Raman active molecules, the partition function Q as expressed by [25]:

$$Q = (2I + 1)^2 \frac{kT}{2B_v}. \quad (6)$$

The g_j is nuclear spin degeneracy, and I nuclear spin quantum number. Differential cross-section for perpendicularly scattered light is [31]:

$$\frac{d\sigma_{J-J'}}{d\Omega} = \frac{64 \pi^4}{45 \epsilon_0^2} b_{J-J'} \frac{\gamma^2}{\lambda_{J-J'}^4}, \quad (7)$$

where the Placzek-Teller coefficient for diatomic molecules $b_{J-J'} = \frac{3(J+J')(J+J'+2)}{8(2J+1)(J+J'+1)}$, and γ^2 is the anisotropy of equilibrium polarizability tensor [33]. For diatomic molecules allowed transitions are $\Delta J = \pm 2$ (positive sign for Stokes and negative sign for anti-Stokes components), whereas all molecular constants for both N_2 and O_2 are given in Table 1.

Table 1. Molecular constants of N_2 and O_2 used in the simulation of the Raman signal [29].

Parameter	N_2	O_2
B_v (eV)	$2.467 \cdot 10^{-4}$	$1.783 \cdot 10^{-4}$
γ^2 ($F^2 m^4$)	$3.95 \cdot 10^{-83}$	$1.02 \cdot 10^{-82}$
g_j (odd/even)	3/6	1/0
I	1	0

In order to detect rotationally resolved Raman spectra transmission Bragg Notch Filter BNF (OptiGrate) was used as a narrow band filter to reduce the Rayleigh scattered light by at least 10^3 times. The laser light at 532 nm was focused with a plano-convex lens of $f=500$ mm 1.5 mm below the nozzle, the same distance as in the case of the Rayleigh scattering spectroscopy. Line integrated scattered signal along of the jet width (radius of 7 mm) was collected with a lens of $f=50$ mm and focused on the fibre of diameter 300 μm . The other end of the fibre was used as a point light source to perform collimation of the scattered light which plays a crucial role for filtration via BNF. Filter BNF-532 is designed in that way that 532 nm light is filtered if the light passes filter by the angle of $6 \pm 1^\circ$. Recently this method of Raman scattering spectroscopy using volume Bragg grating as a notch filter was applied [21, 34]. After passing the filter, the light is collected with a lens and projected to 0.75 m spectrometer Zolix Omni- λ . 1200 grooves/mm grating (blazed on 500 nm) is used to resolve the Raman spectrum with resolution better than 0.11 nm. The spectrum is recorded via ICCD Andor camera synchronised with the laser. The laser energy was set at 20 mJ, and 16000 laser shots were accumulated for each recording of the Raman scattering spectra. The rotational temperature was calculated via a comparison of the experimental spectra with simulation using eq. (3-7). Fitting parameters were the density of the scatterers, the laser energy, resolution of the spectrometer and T_g . Experimental set-up for Raman scattering spectroscopy is exhibited in Figure 2(b). It has to be noted that in comparison with Rayleigh scattering, the method of Raman scattering detection devoid of the disadvantage of results dependence on gas flow dynamics. The method relies on collective inelastic scattering of light by particles and correspondingly an effect of plasma on gas flow is neglected which makes it a perfect candidate to validate Rayleigh scattering. It has to be noted that Raman scattering based calculated temperatures are averaged along the laser line passing through the plasma, and thus only used for validation of the Rayleigh results which also are averaged over the same region of interest. Taking into account the region of averaging of the Raman signal direct comparison of the gas temperature measured by OES method and Raman scattering is not feasible and not considered in current work.

3. Experimental results and discussion

3.1 Electrical characterisation of RF plasma jet

The electrical discharge was sustained by the application of RF forward power in the developed APPJ at a level below 30 W. At RF input power above 30 W, the discharge was transferred to γ -mode. This manifests as highly localised discharge, which is sustained primarily by a secondary emission of the electrons from hot contact spot-localised to one of the electrodes. Through this work only α -mode uniform discharge was studied. The discharge is formed at the lowest power just on the edge of the electrodes. The increase of the power to 30 W leads to expansion of the discharge, propagating over the whole length of the electrode which is 10 mm long as indicated in Figure 1. Similar expansion of the RF plasma has been also noticed in our previous work on co-planar RF plasmas [35]. Further increase of the power leads to the discharge transformation to γ -mode. In α -mode at power of 30 W the discharge is filling the whole area between the electrodes. The V-I characteristics of the discharge are presented in Figure 3(a) Power dissipation in the discharge when plasma is off and on is shown in Figure 3(b) based on methodology described in [36]. According to measurements the plasma source stable operating range is from 10 W (minimum RF power to sustain plasma) to 30 W (γ -mode transition). In the case of adding nitrogen/air to the gas flow, due to optical emission spectroscopy measurements, the α -mode is still in the range of power from 13 W to 30 W. Length of the visible effluent depends on power (see Figure 1.) and it is in the range of 2.5 - 5 mm, which corresponds to a minimum and maximum power. An example of the discharge appearance in α - and γ -mode is presented in onsets in Figure 3.

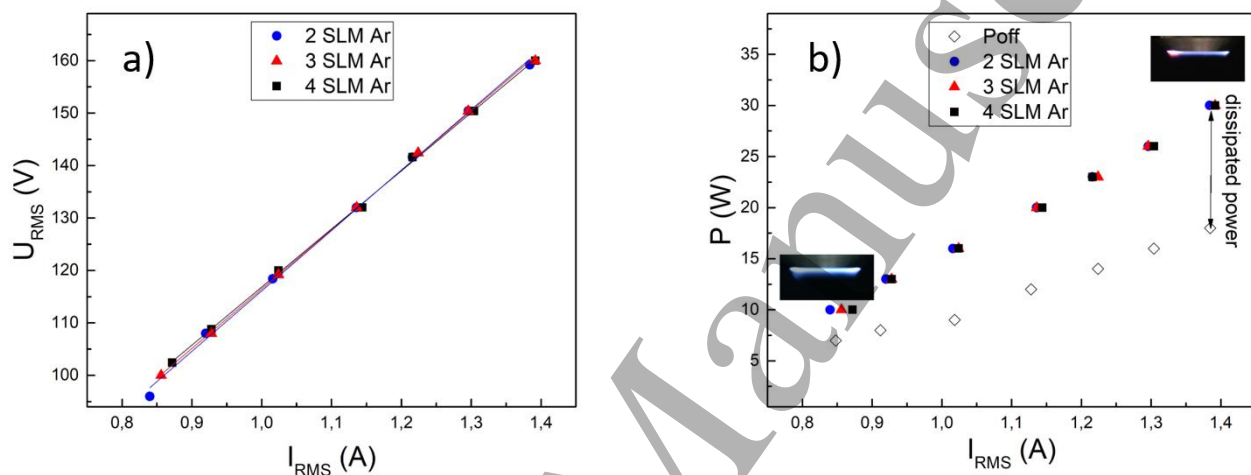


Figure 3 Electrical characterisation of RF jet (a). I-V characteristics of the RF plasma jet operating in α -mode recorded with increasing the RF forward power from 10 to 30 W; (b) Forwarded power with gas flow, and forwarded power without gas flow (P_{OFF}) as a function of the current, with a visual representation of the discharge in α - and γ -mode.

It is interesting to note that an increase in the gas flow rate from 2 to 4 slm has very little impact on the electrical characteristics of the plasma source. However, at a flow rate above 4 slm the discharge sustaining in a stable regime is not possible and plasma randomly completely extinguished or transferred to γ -mode. There is a small increase of V_{RMS} value for lowest power range from 96 to 102 V with an increase in the flow rate from 2 to 4 slm. However, the current of the jet in α -mode is independent of the gas flow, with current density in the range of 0.2-0.37 A/cm² for all working powers. Considering almost linear V-I characteristic of the discharge with a positive slope of 110 V/A it can be expected that the plasma operates in the glow-like mode sustained by Ohmic electrons heating [37]. This indicates that the main ionisation processes are driven by fast electrons accelerated in oscillating RF field [38]. Sustained RF glow discharge is characterised by constant V/I phase difference of about 88° that implies on the stability of α -mode and discharge capacitive character. The reason for a slight deviation of -2° from the pure capacitive coupling is due to decreasing capacitive contribution and increase of the resistive one with an increase of the power similar to observations of others [39, 40]. A observation of stable α -mode formation in argon plasma has been also found for plasma jet described in [41]. The evolution of plasma constituents during an RF cycle was experimentally studied by use of fast imaging of the discharge emission presented in Figure 4. For this purpose, the fast imaging camera was used with a maximum transparent filter at 750 nm, which corresponds to Ar I transition $4p(^2P^0_{1/2}) \rightarrow 4s(^2P^0_{1/2})$. This is an excited state with a radiative lifetime of $\tau \approx 22$ ns [42], which is reduced to less than 5 ns due to quenching at high pressures. This intensive line is therefore suitable for RF imaging because the lifetime of atoms in excited levels is shorter than the duration of the RF cycle of 73 ns and so the emission of Ar I should be directly related to the electron kinetics in the discharge. Emission of OH $A^2\Sigma^+ \rightarrow X^2\Pi_i$ transition was also recorded but no temporal evolution within RF cycle is noticed due to longer radiative lifetime of OH radicals $\tau \approx 0.6-0.7$ μ s. Imaging of APPJ, presented in Figure 4(a, b) was performed for five different time points during the RF cycle corresponding to applied voltage: $V_{RF} = 0$ ($T_1 = 0$ ns), $V_{RF} = +V_0$ ($T_2 = 18,44$ ns), $V_{RF} = 0$ ($T_3 = 36,87$ ns), $V_{RF} = -V_0$ ($T_4 = 55,3$ ns) and $V_{RF} = 0$ ($T_5 = 73,74$ ns). The imaged bulk plasma was uniform in all the time frames, whereas the formed sheath exhibited a strong emission near the RF electrode. The sheath width is calculated from the image corresponding to the highest argon emission near the RF electrode when its voltage reaches a

negative amplitude as indicated in Figure 4(b). The sheath is here considered to be a width of the illuminating zone near the electrode where Ar I emission drops by 90% from the peak intensity I_{peak} . Moreover, the RF imaging is indicating a higher intensity of Ar I lines in the electrode area (sheaths) with respect to the bulk plasma (Figure 4.). The length of the developed sheath, corresponding to time 55.4 ns, is estimated to be around 200 μm which is well in agreement with results of particle-in-cell (PIC) simulation of RF plasmas operating at high current [43].

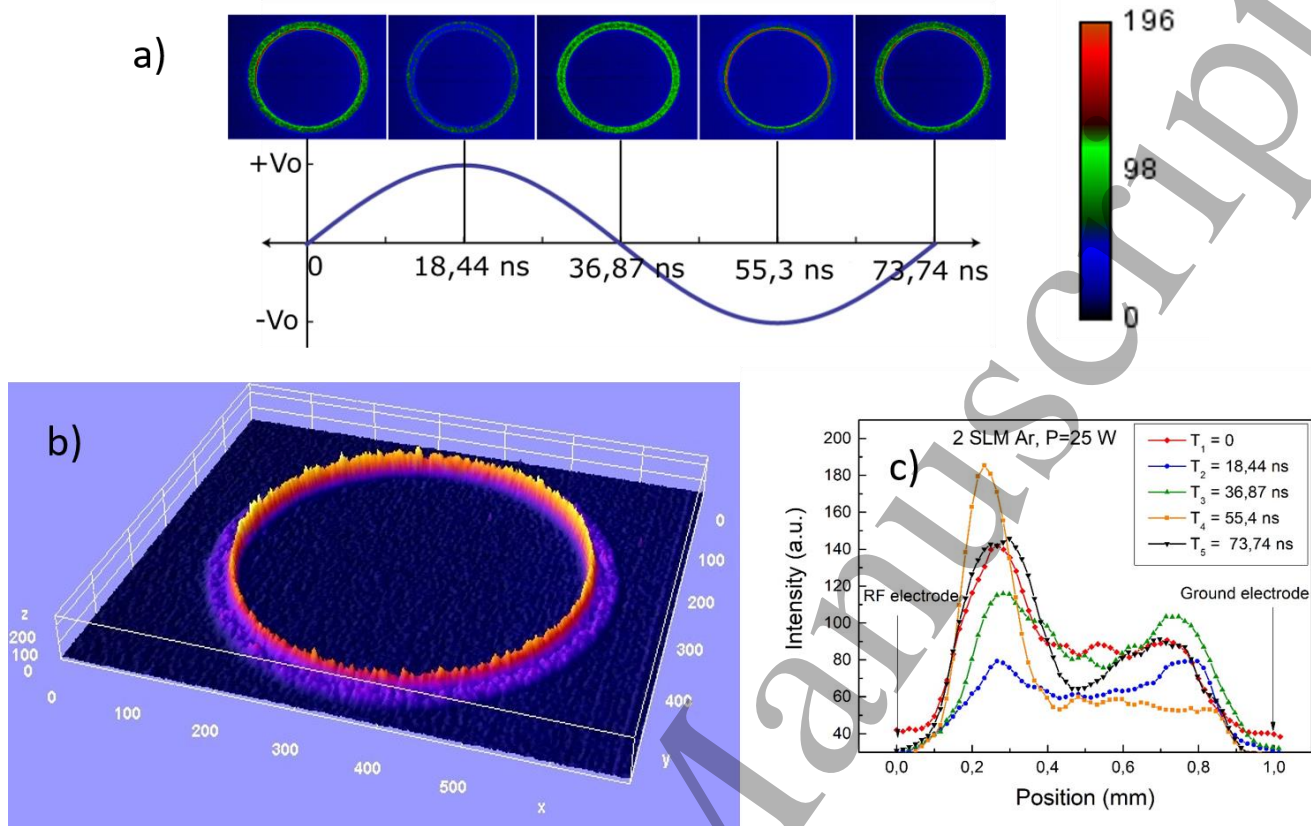


Figure 4. Time-resolved imaging of the RF APPJ with 5 ns exposure time in single-shot mode: a) The images are recorded through a bandpass filter of 10 nm FWHM centred at 750 nm that corresponds to Ar I emission. Time of the records is indicated in the offsets; b) 3D map of intensity for a case of 55.4 ns time frame with an indication of the sheath formed near powered electrode; c) intensity distribution in the inter-electrode gap and near RF powered and ground electrodes

It should be noticed that in a contrast to symmetrical sheath formation observed in PIC simulation, the sheath in APPJ is strongly asymmetrical with a barely visible sheath formed at the ground electrode (virtual cathode at 18.4 ns) and very strong sheath at RF powered electrode (virtual cathode at 55.4 ns). Stronger light emission on the RF electrode is also noticed in our earlier work with RF planar discharge [44]. This effect is partially explained by the fact that the APPJ electrodes system is asymmetrical with a 5:6 ratio of electrode areas. However, the area ratio of the electrodes cannot explain fully the observed strong asymmetry of the discharge. Correspondingly other processes, unknown at the moment, can have important contribution to the asymmetry and additional research is required which is out of the scope of this work. The presence of the sheath in RF plasma can have strong impact on stabilisation of the discharge and generation of uniform α -mode plasma without filaments or transition to γ -mode.

Opposite to atmospheric pressure DBDs sustained in kHz frequency range in Ar which usually operate in filamentary mode, our APPJ is a uniform-stable plasma operating in diffuse α -mode. This is obviously an advantage of the source especially in terms of biomedical treatments. Operation of the discharge in diffuse α -mode requires a mechanism to stabilise the discharge and suppress heating instabilities which otherwise would result in the transition of the discharge to γ -mode of operation. Sustaining of the source is analysed based on the balance between processes of dissociation/recombination and diffusion of ions Ar_2^+ and electrons in the bulk of the discharge [45]. In a case when recombination processes are dominant, the steady α -mode switches to filamentary γ -mode sustained by the secondary electron emission from the electrodes. If processes of diffusion are dominated over recombination, then one can conclude that the heating dissipation is suppressed and uniform α -mode is realised. In a self-sustained low ionisation degree discharges, as one studied here, a major loss of the input RF power P dissipated in the discharge of volume V is because of elastic processes. Correspondingly, the electron density in the bulk is estimated using power balance for free electrons in plasma assuming only elastic collisions as [46]:

$$\frac{P}{V} = n_e \cdot n_{Ar} \cdot \frac{3m_e}{m_{Ar}} \cdot k_{el} \cdot T_e . \quad (8)$$

In eq. (8) the term responsible for heating of the gas is neglected as T_g is much lower in comparing with T_e .

Parameters n , m , T are the density, mass, and temperatures of species, respectively. Coefficient k_{el} stands for the rate coefficient of elastic collisions between electron and argon atoms obtained from BOLSIG+ for characteristic electric fields E/N 1, 5, 10, 50 and 100 Td ($1\text{Td}=10^{-21} \text{Vm}^2$). Maximum energy density is considered as 30MW/m^3 based on the results presented in Figure 3(b). On the other hand, the self-sustaining operation of the discharge should fulfil the ionisation/ recombination balance [33]:

$$10^{-14} n_e n_{Ar} e^{\frac{E_i}{kT_e}} = n_+ n_e k_d . \quad (9)$$

Here k_d stands for dissociative recombination rate and is typical of $10^{-14} \text{m}^3\text{s}^{-1}$ [39]. Considering the condition of quasineutrality eq. (9) is simplified to the ionisation balance equation:

$$n_e = n_{Ar} e^{\frac{E_i}{kT_e}} , \quad (10)$$

where E_i is the first ionisation energy of Ar_2 as Ar_2^+ is a dominant molecular ion APPJ at atmospheric pressure. Dependence of electron density on T_e for the range of characteristic values for atmospheric pressure plasmas (few eV) is presented in Figure 10, indicating the steady-state value for $n_e=3.2 \cdot 10^{18} \text{m}^{-3}$ and $T_e=1 \text{eV}$ for the experimental condition of 5 Td. This very rough estimation of plasma parameters is in good agreement with previous works of our group based on COMSOL simulation and continuum radiation calculations [44, 47].

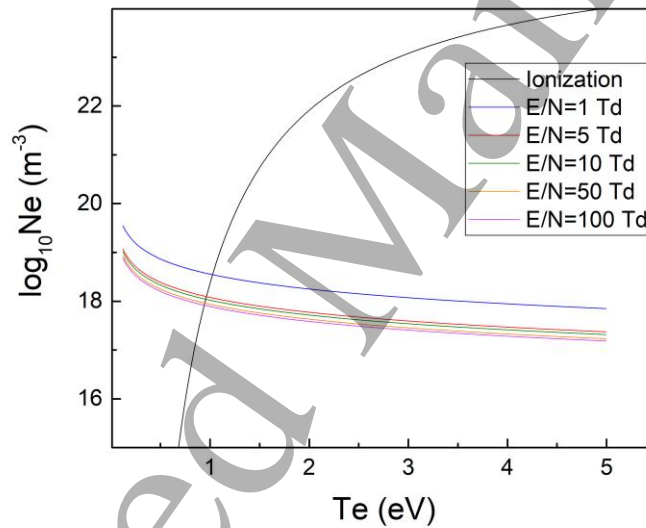


Figure 10. Electron density and temperature estimation plots from power and ionization/recombination balance. Curves for reduced E/N in the range 1-100 Td represents power balance due to elastic collisions.

The results of power and ionisation/recombination balance can be used to estimate characteristic times for both diffusion and recombination of charged particles. Obviously, in the high-pressure plasmas, the dominant processes of charge particle loss are dissociative recombination of electrons with Ar_2^+ ions and diffusion of particles from the bulk [39]. The dissociative recombination described as $\text{Ar}_2^+ + e^- \leftrightarrow \text{Ar} + \text{Ar}$ has a characteristic time given as:

$$\tau_{diss} = \frac{1}{n_e k_{e-i}} , \quad (11)$$

where k_{e-i} is a coefficient describing the electron-ion recombination. On the other hand, characteristic time for argon cluster ions to leave plasma due to diffusion can be expressed as:

$$\tau_{diff} = \left(\frac{l}{2.4}\right)^2 \cdot \frac{e}{\mu k T_e} , \quad (12)$$

where l is characteristic diffusion length and μ is Ar_2^+ mobility in argon [41]. Calculations, with the use of n_e and T_e , estimated from Figure 10, indicate that τ_{diss} is close to 4.5 μs . This is about 30-times faster than diffusion processes with $\tau_{diff} \sim 140 \mu\text{s}$. Such a large difference in between τ_{diff} and τ_{diss} should lead to thermal instabilities and transfer of the RF discharge to γ -mode. This is contradictory with experimental results and leads to the conclusion that another process of RF discharge stabilisation should exist [48]. Both estimations of τ_{diff} and τ_{diss} are made for the bulk plasma. In contrast to DBDs or pulsed plasmas operating at high pressure, the sheath regions near the electrodes are formed in the RF APPJ as presented in Figure 4. The sheath plays an important role in discharge sustaining and can stabilize α -mode regime. High electrical potential in the sheath repels fast electrons directing them to the bulk. PIC simulation of Lieberman *et al.* [43] has demonstrated electron density decrease in the sheath, and sheath behaviour even at high pressure is similar to Child-Langmuir sheath in a low pressure capacitively coupled RF discharges. Decrease of n_e affects processes of dissociation/recombination lead to an increase of τ_{diss} . On the other hand PIC simulation exhibits a high reduced field E/N in sheaths estimated to be up to 1 MV/m [43]. This results in an increase of ion mobility which causes a decrease of τ_{diff} and leads to discharge stabilisation in the sheath, where condition $\tau_{diff} \sim \tau_{diss}$ is reached. The sheath effect in a stabilisation of the RF APPJ is important for sustaining the discharge in a uniform mode that is a key issue for the generation of low-temperature active media for the biomedical application of the plasmas.

3.2 Temperature characterisation by OES method

The RF source presented in this study was developed for the purpose of trans-epidermal drug delivery. In respect to its targeted application, the source requires to fulfil; (i) a safe operation without initiating thermal damage to the tissue in a contact with plasma, (ii) the compatibility with aerosol injection, and (iii) the ability of a large area treatment. Among different plasma properties, the gas temperature is considered to pose a key parameter for its application. To this end, a well-known technique based on OES gas temperature measurements was applied. The method is based on rotational temperature calculations of OH $\text{A}^2\Sigma^+ \rightarrow \text{X}^2\Pi_1$ (0,0) and $\text{N}_2 \text{C}^3\Pi_u \rightarrow \text{B}^3\Pi_g$ (0,2) molecules from the partially resolved ro-vibrational bands. In the first case, T_g was measured in the power range of 10 W - 30 W for Ar flow of 2, 3, and 4 slm from OH partially rotationally resolved band. The LIFBASE simulation and its comparison of the measured spectra are presented in Figure 5(a). In the second case, the N_2 transition $\text{C}^3\Pi_u \rightarrow \text{B}^3\Pi_g$ (0,2) was used for rotational molecular temperature calculation which is based on MassiveOES software [49] where only linear part of the Boltzmann plot has been taken into account similar to [22]. The Boltzmann plot for J numbers in the range of 4-20 was used for the analysis of N_2 radiation and obtained from the Boltzmann plot slope temperature is presented in Figure 5(b).

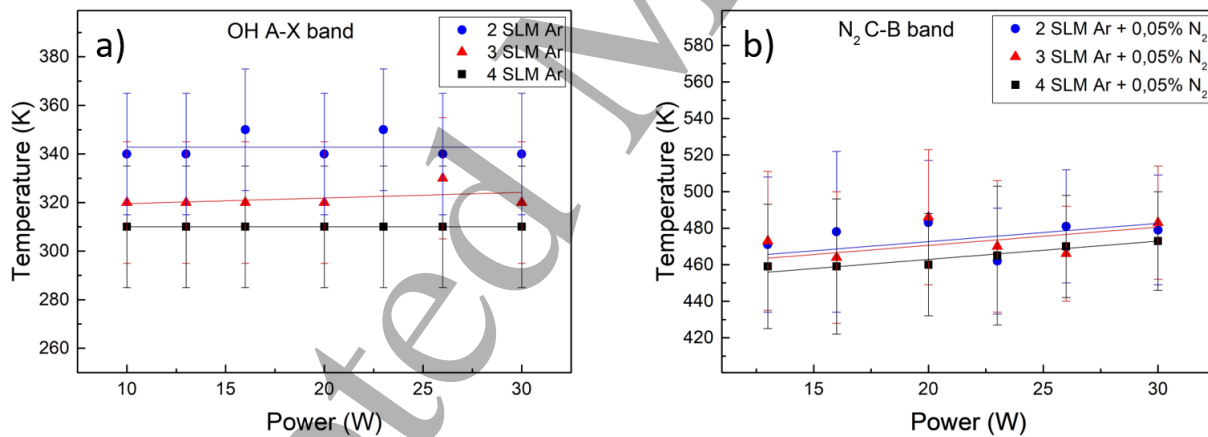


Figure 5. The gas temperature in plasma calculated via (a) LIFBASE software fitting of OH (A-X) band for different gas flow and RF forward power; (b) calculated via Boltzmann plot of N_2 transition (C-B) with the use of MassiveOES [49]

The OH rotational temperature of the effluent of Ar plasma which propagates into the ambient air was estimated to be in a range of 310 - 350 K, at a distance of 1.5 mm from the nozzle. Interestingly, the RF power increase had a negligible impact on the rotational temperature of OH(A) radicals, which is in agreement with previous results from our group [35]. This is explained by the increase of RF power in α -mode which results in plasma expansion between the electrodes along with the gas flow, and the effluent that leads to almost constant power density W/cm^3 [35]. OES measurements presented in Figure 5(a,b) are line-of-sight integrated across the effluent correspondingly providing the spatially averaged value of T_g . In the case of N_2 admixing up to 0.2%, no change in visual appearance or V-I characteristic of the discharge was detected. However, the rotational temperature estimated from the linear slope of the Boltzmann plot indicates T_g in the range of 450-480 K. It has to be noted that N_2 distribution shows Boltzmann behaviour for rotational levels up to $J=20$ with the temperature indicated in Figure 5(b). Whereas the fitting the vibrational band 0-2 with J numbers up to 32 leads to unrealistically high rotational temperature of 580-680 K. Correspondingly, only the range of rotational numbers $J=4-20$ with linear Boltzmann slope was analysed. The results of Figure 5 indicates a discrepancy between T_g obtained from OH

(A-X) emission and $N_2(C-B)$. Moreover, there was almost no tendency in T_g as a function of gas flow in case of use N_2 band emission. In number of studies [16, 23] it was indicated that often encountered issue in non-equilibrium plasmas is the energy transfer from argon metastable atoms in $Ar(^3P_2)$ and $Ar(^3P_0)$ states to $N_2(X)$ producing electronically excited $N_2(C)$ molecules, which are not in equilibrium with the rest of the molecules. As this reaction is a near resonance process, then it is often a dominant production mechanism of N_2 excited states in Ar discharges with small additions of N_2 or air [16]. The effect of Ar metastable energy transfer to N_2 species is noticeable by introducing N_2 to feeding gas as shown in Figure 6. With the addition of N_2 to the working gas there is an increase in the intensity of nitrogen lines (second positive system) and reduction of argon lines from transition 4p-4s. This behaviour can be related to an efficient energy transfer from argon excited states to nitrogen species inducing overpopulation of $N_2(C)$ level and so non-Boltzmann distribution.

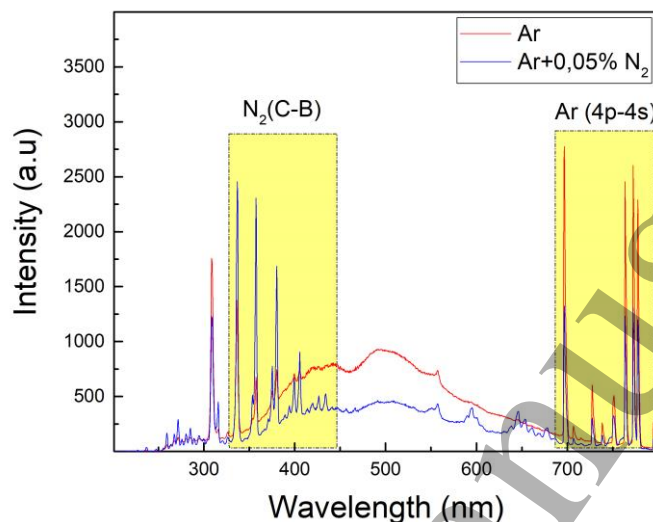
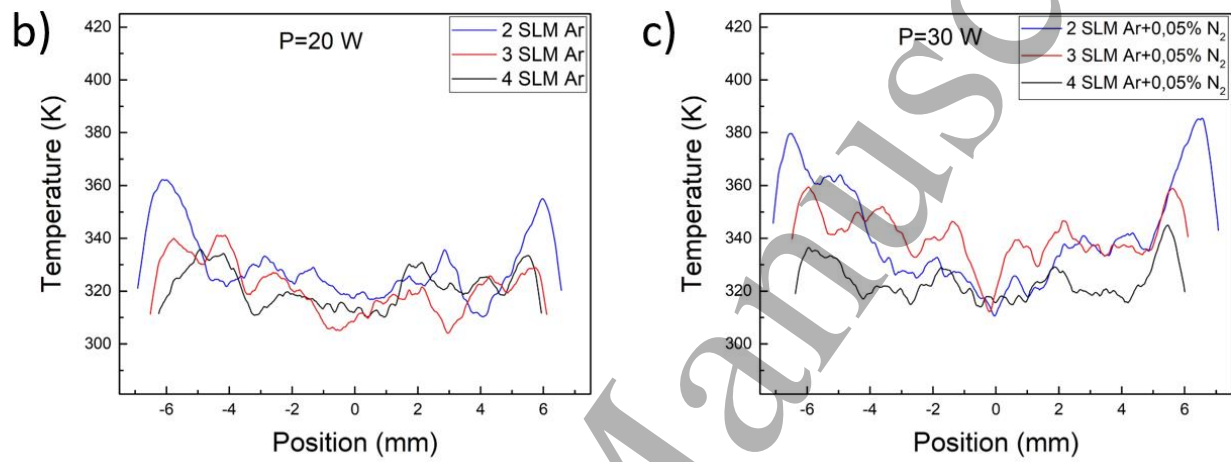
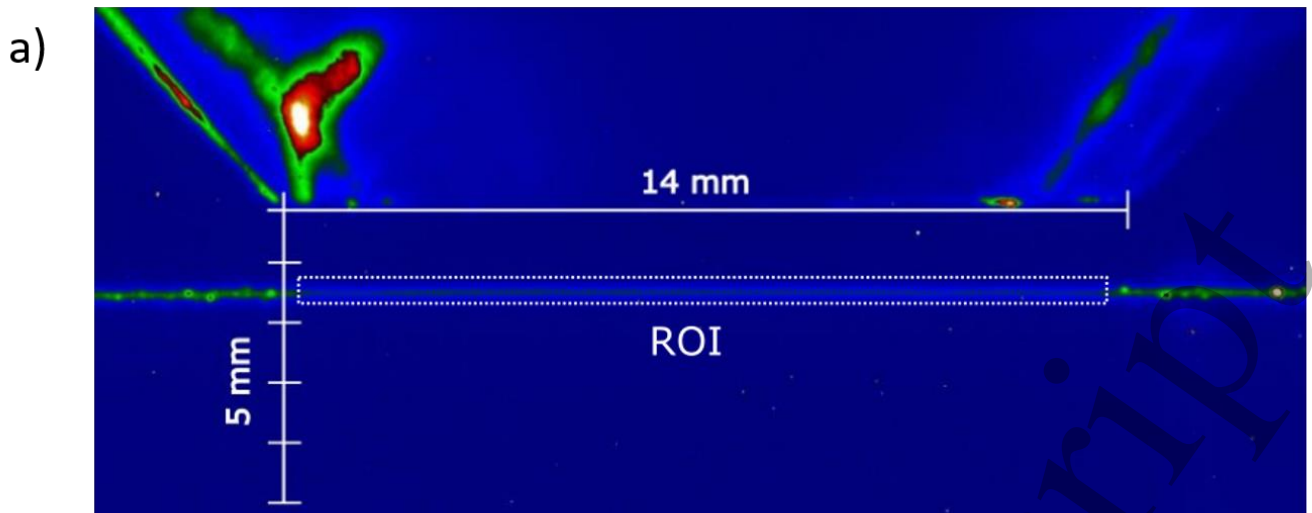


Figure 6. Example of RF APPJ spectra in pure argon (red), and argon in mixture with 0.05% of nitrogen (blue).

This fact can lead to the overestimation of gas temperature from N_2 band. This could be then a reason for the discrepancy of results in our study. On the other hand, the use of OH(A-X) emission as a proper indicator of T_g is also very questionable [22, 50], and has to be revalidated based on direct methods of neutrals translation temperature detection. To this end, the two other methods based on laser scattering detection are applied. However, it has to be noted that the laser scattering methods presented in section 3.3 are more experimentally demanding and have other number of limitations, e.g. cannot be applied in a case when an aerosol is injected into plasma. For this reason, we used them only for validation of the OES results and unrevealing insights into the gas heating inside the RF plasma jet.

3.3 Temperature characterisation by the laser scattering.

The Rayleigh scattering allows direct measurement of gas density proportional to T_g through eq. (2) with a high spatial and temporal resolution. A typical example of the Rayleigh scattering image taken with the ICCD camera in pure Ar plasma of 10 W at 1.5 mm distance from the nozzle is given in Figure 7(a). Only part of the signal free of Mie scattering, indicated by dotted area ROI in Figure 7(a), was analysed hereinafter. No laser synchronisation with RF voltage was applied as no temporary dependence of T_g is expected because of the characteristic time of RF signal (~ 74 ns) is too short for gas heating to follow the RF cycle. Spatially resolved gas temperatures in Ar and Ar+ N_2 plasma effluent are presented in Figure 7(b,c) for a case of RF power of 20 and 30 W in Ar and Ar+ N_2 mixtures, respectively. Based on the spatially resolved profile of T_g it can be assumed that gas temperature is constant along of the jet radial cross-section at power below 20 W. Higher T_g in a position that corresponds to space between the electrodes was noted at higher power as indicated on Figure 7(b). Small asymmetry of the temperature profiles what can be seen in Figure 7(b,c), is explained by very small misalignment of the electrodes what results in the shorter gap and correspondingly more intensive discharge in that location. This effect was also observed during fast imaging (see Figure 4. time frame 55.4 ns bottom part of the inter-electrode gap).



33 **Figure 7.** Rayleigh scattering of the laser light of 532 nm at 1.5 mm distance from the nozzle. a) The image was taken with an ICCD
34 camera of the laser beam passing through Ar plasma for $P=10$ W. The dotted area represents the region free of Mie scattering and
35 only this region was analysed for the temperature estimations; b) Spatially resolved temperature measurements via Rayleigh
36 scattering (Ar gas) at plasma power of 20 W; c) Spatially resolved temperature measurements via Rayleigh scattering (Ar+N₂ gas)
37 at plasma power of 30 W.

38
39
40
41 The Rayleigh radial resolved signal presented in Figure 7(b) was averaged along the regions corresponding to plasma effluent
42 formed in the inter-electrode area, e.g. a region of 1 mm width located at the position from 6 to 7 mm for 2 slm flow. It has to be
43 emphasized that position of the maximum of the gas temperature depends on the gas flow and a shift towards inner-electrode region
44 was observed with an increase of the flow as shown in Figure 7. Due to the shift of the high temperature region the area of the
45 Rayleigh signal averaging has been adjusted depending on the flow keeping the width of the averaging at 1 mm. Described
46 methodology of the Rayleigh signal averaging was applied in order to determine space averaged T_g which can be directly compared
47 with OES measurements presented in section 3.2. Obtained results for both Ar and Ar+N₂ mixtures as a function of gas flow rate
48 and forward RF power are exhibited in Figure 8. Temperature profile analysis shows uniform temperature distribution at the lowest
49 power of 10 W. With increasing input power, higher temperature region corresponding to the effluent region starts to be noticeable,
50 as shown in Figure 7(b,c). As expected the highest temperature difference is for the lowest flow. With increasing of flow, a shape
51 of the effluent is more conical and there is effective heat transfer towards middle of the plasma jet leading to thermalization and
52 more uniform temperature profile.
53
54
55
56
57
58
59
60

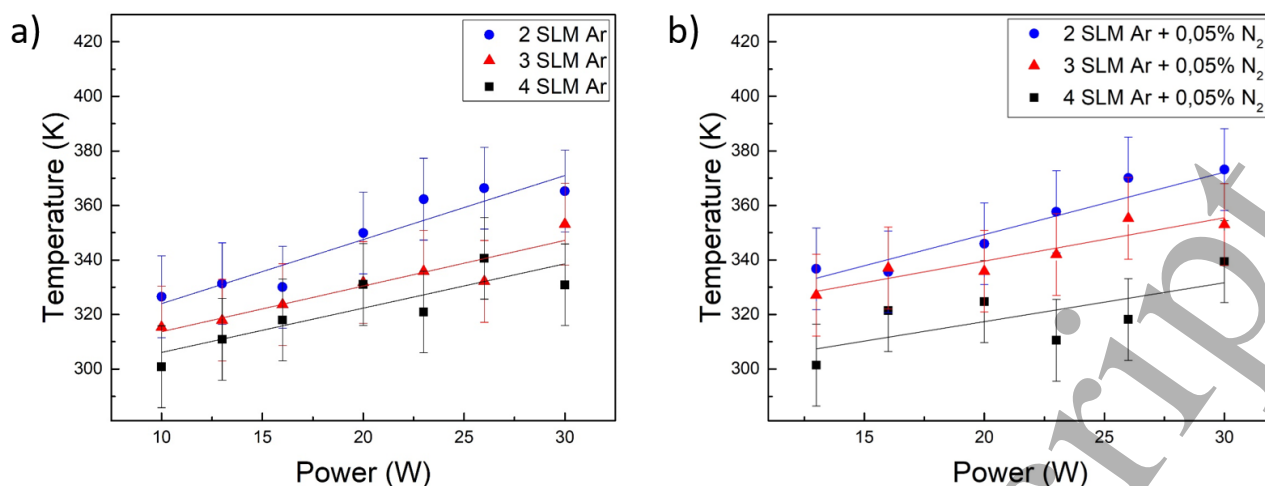


Figure 8. The gas temperature T_g that corresponds to the inter-electrode region analysed through the averaging the Rayleigh scattering signal in a) Ar gas; b) Ar+N₂ mixture.

Obtained results indicate that T_g in both Ar and Ar+0.05% N₂ plasma is in the range of 300-370±15 K, depending on applied flow and power. Figure 7(c) confirms an approximation of negligible impact of the N₂ admixing used for OES experiments on T_g . The method of Rayleigh scattering has higher sensitivity in comparing to OES and T_g can be estimated with an uncertainty of ±15 degrees. This allows seeing an effect of input RF power on gas temperature which was undetectable in OES measurements. As presented in Figure 8(a,b), the RF power increase results in an almost linear increase in gas temperature of the effluent. The maximum increase of temperature was found for the smallest flow rate of Ar gas due to less effective heat transfer at 2 slm. Radial averaged value of T_g measured by the Rayleigh scattering is in a very good agreement with the OES method based on OH(A-X) emission. On the other hand, disagreement with results obtained through the use of N₂ emission is almost 100 K for all conditions. This leads to a conclusion of strong overestimation of T_g in a case of utilisation of emission of the second positive system of N₂ for determination of T_g .

Despite the good agreement of the Rayleigh scattering results and OES method based on OH(A-X) emission, the elastic laser scattering is not free of well-known intrinsic problem: the scattering is dependent on the species density, and so it requires the validity of a condition that gas flow dynamics is not affected by plasma. In this work, the aforementioned problem was checked, and an effect of the gas flow dynamics on elastic scattering was validated by inelastic Raman scattering of the laser light on N₂ and O₂ molecules appearing in the effluent due to ambient air diffusion. Raman spectrum was measured in Ar plasma with 0.2% admixing of molecular gas (air) at a position of 1.5 mm beneath the nozzle. It has to be noted that due to the Bragg grating used to filter out the Rayleigh line at 532 nm, the detection scheme presented in Figure 2(b) has a low radial resolution. To this end spatially averaged Raman signal was detected and compared with the Rayleigh scattering results. As mentioned earlier, Raman signal based gas temperature was only used to validate applicability of the Rayleigh scattering method in order to clarify the effect of the discharge on the gas flow dynamics. Accordingly, spatially averaged Raman signal over the region indicated as ROI in Figure 7(a) was used as an indicator of the average temperature of the plasma jet effluent and was compared with Rayleigh scattered signal averaged over the same length.

The strongest influence of plasma on gas flow dynamics is expected at the lowest gas flow and high power. Due to this reason, the Raman spectroscopy was performed at 2 slm Ar flow. In order to calculate T_g from Raman spectra, theoretical Raman spectra were fitted to experimental results with input parameters: the resolution of the spectrometer, N₂ and O₂ density, and T_g . Both anti-Stokes and Stokes signals were observed but due to the stronger Stokes signal, only this part of the Raman spectra was analysed. The experimental and fitted Stokes components of Raman spectra are presented in Figure 9.

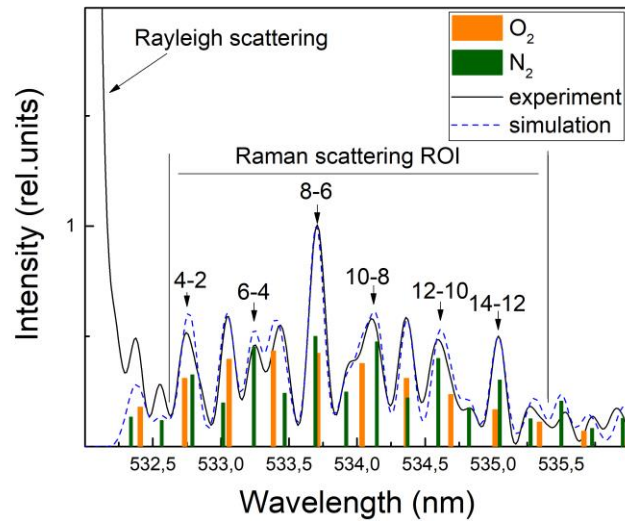


Figure 9. Example of normalised experimental and simulated Raman spectra (Stokes component) for Ar plasma with 0.2% molecular gas admixing for RF forward power of 15 W. Raman components attributed to O₂ and N₂ are presented with red and green colour with an indication of the rotational numbers of the lines.

During experiments, it was found that the first 3 lines in Stokes components with $J \leq 3$ were partially affected by strong Rayleigh signal which was still presented even after filtration by single BNF-532 filter. All 3 lines were excluded from the fitting procedure as well as lines above 535.2 nm (corresponding to $J > 14$) as S/N ratio was too low for high J number lines due to low lines intensity. The Raman spectrum fitting indicates T_g of 320 ± 25 K for 15 W RF power which is in good agreement with the Rayleigh scattering result of 330 ± 15 K obtained by averaging the scattered signal over the ROI -7 to +7 mm, indicated in Figure 7(a). Considering good agreement between Rayleigh and Raman spectroscopy results it can be concluded that RF discharge in α -mode does not affect the dynamics of the gas flow and method of Rayleigh scattering is applicable to similar plasmas.

As a summary, the rotational temperature measured by emission of OH(A) band well represents the gas temperature evaluated by the direct detection of Rayleigh scattering. The method based on emission spectroscopy of ro-vibrational bands of OH radicals can be used in future tests of the developed source in biomedical tests and treatment of skin surfaces where applicability of other methods is technically challenging.

5. Conclusions

Annular-shape radio-frequency atmospheric pressure plasma jet was characterised with electrical and temperature diagnostics. The plasma device is designed for biomedical application in wound healing and topical drug delivery with the possible aerosol introduction through a hollow inner-electrode. For this reason, the aim was to obtain uniform and cold plasma in order to prevent any damages to the skin. The obtained results showed that this can be achieved with RF capacitive-coupled discharge operating in a uniform diffuse α -mode at RF power below 30 W. In order to explain the stability of a uniform α -mode of the discharge, processes of diffusion and recombination were analyzed. It is proposed that stabilization of the discharge operation in α mode is achieved due to the presence of the sheath.

Gas temperature in plasma is determined using OES technique based on rotational temperature of OH radicals $A^2\Sigma^+ \rightarrow X^2\Pi_1$ (0,0) band and N₂ $C^3\Pi_u \rightarrow B^3\Pi_g$ (0,2) band. The temperature obtained by the fitting method of OH $A^2\Sigma^+ - X^2\Pi$ (0,0) band indicated T_g of 340, 320 and 310 K for the flow of 2,3 and 4 slm of Ar. Considering safety limit of the source applicability of 333 K (60^o C), for short treatment time, it can be concluded that operational range of the APPJ is limited by flow rate above 2 slm in case of α mode. However, the measurements for N₂ and OH bands yield discrepant results of almost 100 K, where the highest temperatures of 450-480 K are obtained in the case of N₂. For this reason, the temperature measurements by OES technique were revalidated by two other independent techniques based on laser scattering. Rayleigh scattering has shown uniform temperature distribution at RF forwarded below 20 W while at higher powers inner-electrode region is noticeable for low flow. For higher flow then 2 slm mixing with middle part starts to be significant, thermalization occurs and temperature distribution is close to uniform. Radially averaged T_g determined by Rayleigh method is in a good agreement with OH temperature determined by emission spectroscopy. The assumption of negligible effect of plasma ignition on gas flow dynamics and so on results of the Rayleigh scattering has been validated by Raman scattering. It was revealed that both methods agree well with OES results based on OH (A-X) measurements. Low gas temperature of the RF plasma source combined with uniform and diffuse afterglow and possibility of the source coupling

with aerosol injection is considered to be beneficial for variety of biomedical application including topical drugs injection and wound healing.

6. Acknowledgements

The research work performed was supported by the FWO/ARRS agencies project “Plasma-skin interactions: from wound treatment to topical introduction of molecules”, numbers G084917N and N3-0056, respectively.

7. Reference list

1. Penkov, O.V., et al., *A review of recent applications of atmospheric pressure plasma jets for materials processing*. Journal of Coatings Technology and Research, 2015. **12**(2): p. 225-235.
2. Tendero, C., et al., *Atmospheric pressure plasmas: A review*. Spectrochimica Acta Part B-Atomic Spectroscopy, 2006. **61**(1): p. 2-30.
3. Weltmann, K.D. and T. von Woedtke, *Plasma medicine-current state of research and medical application*. Plasma Physics and Controlled Fusion, 2017. **59**(1): p. 11.
4. Weltmann, K.D., et al., *Atmospheric-pressure plasma sources: Prospective tools for plasma medicine*. Pure and Applied Chemistry, 2010. **82**(6): p. 1223-1237.
5. Isbary, G., et al., *Non-thermal plasma—More than five years of clinical experience*. Clinical Plasma Medicine, 2013. **1**(1): p. 19-23.
6. Von Woedtke, T., H.R. Metelmann, and K.D. Weltmann, *Clinical plasma medicine: state and perspectives of in vivo application of cold atmospheric plasma*. Contributions to Plasma Physics, 2014. **54**(2): p. 104-117.
7. Winter, J., R. Brandenburg, and K.D. Weltmann, *Atmospheric pressure plasma jets: an overview of devices and new directions*. Plasma Sources Science & Technology, 2015. **24**(6): p. 19.
8. Park, G.Y., et al., *Atmospheric-pressure plasma sources for biomedical applications*. Plasma Sources Science & Technology, 2012. **21**(4): p. 21.
9. Selwyn, G., et al., *Materials Processing Using an Atmospheric Pressure, RF-Generated Plasma Source*. Contributions to Plasma Physics, 2001. **41**(6): p. 610-619.
10. Niemi, K., V. Schulz-Von Der Gathen, and H. Döbele, *Absolute atomic oxygen density measurements by two-photon absorption laser-induced fluorescence spectroscopy in an RF-excited atmospheric pressure plasma jet*. Plasma Sources Science and Technology, 2005. **14**(2): p. 375.
11. Brandenburg, R., *Dielectric barrier discharges: progress on plasma sources and on the understanding of regimes and single filaments*. Plasma Sources Science and Technology, 2017. **26**(5): p. 053001.
12. Wang, S., V. Schulz-Von der Gathen, and H. Döbele, *Discharge comparison of nonequilibrium atmospheric pressure Ar/O₂ and He/O₂ plasma jets*. Applied physics letters, 2003. **83**(16): p. 3272-3274.
13. Schutze, A., et al., *The atmospheric-pressure plasma jet: a review and comparison to other plasma sources*. IEEE transactions on plasma science, 1998. **26**(6): p. 1685-1694.
14. Laux, C.O., et al., *Optical diagnostics of atmospheric pressure air plasmas*. Plasma Sources Science & Technology, 2003. **12**(2): p. 125-138.
15. Sarani, A., A.Y. Nikiforov, and C. Leys, *Atmospheric pressure plasma jet in Ar and Ar/H₂O mixtures: Optical emission spectroscopy and temperature measurements*. Physics of Plasmas, 2010. **17**(6): p. 8.
16. Bruggeman, P.J., et al., *Gas temperature determination from rotational lines in non-equilibrium plasmas: a review*. Plasma Sources Science & Technology, 2014. **23**(2): p. 32.
17. Murphy, A. and A. Farmer, *Temperature measurement in thermal plasmas by Rayleigh scattering*. Journal of Physics D: Applied Physics, 1992. **25**(4): p. 634.
18. Van Gessel, A., et al., *Laser scattering on an atmospheric pressure plasma jet: disentangling Rayleigh, Raman and Thomson scattering*. Plasma Sources Science and Technology, 2012. **21**(1): p. 015003.
19. Kuhn, M., et al., *Plasma actuators for active flow control based on a glow discharge*, in *14th High-Tech Plasma Processes Conference*, D. Uhrlandt, P. Teulet, and J. Schein, Editors. 2017, IOP Publishing Ltd: Bristol.
20. Neretti, G., A.C. Ricchiuto, and C.A. Borghi, *Measurement of the charge distribution deposited by an annular plasma synthetic jet actuator over a target surface*. Journal of Physics D-Applied Physics, 2018. **51**(32): p. 9.
21. Klarenaar, B.L.M., et al., *A rotational Raman study under non-thermal conditions in a pulsed CO₂ glow discharge*. Plasma Sources Science & Technology, 2018. **27**(4): p. 12.

22. Bruggeman, P., et al., *Characterization of a direct dc-excited discharge in water by optical emission spectroscopy*. Plasma Sources Science & Technology, 2009. **18**(2): p. 13.
23. Sobolev, N., *Electron-excited molecules in a nonequilibrium plasma*. Moscow Izdatel Nauka, 1985. **157**.
24. Miles, R.B., W.R. Lempert, and J.N. Forkey, *Laser Rayleigh scattering*. Measurement Science and Technology, 2001. **12**(5): p. R33-R51.
25. Snee, M. and W. Ubachs, *Direct measurement of the Rayleigh scattering cross section in various gases*. Journal of Quantitative Spectroscopy & Radiative Transfer, 2005. **92**(3): p. 293-310.
26. deRegt, J.M., et al., *Air entrainment in an inductively coupled plasma measured by Raman and Rayleigh scattering*. Spectrochimica Acta Part B-Atomic Spectroscopy, 1996. **51**(12): p. 1527-1534.
27. Brehmer, F., et al., *Gas temperature in transient CO₂ plasma measured by Raman scattering*. Journal of Physics D-Applied Physics, 2015. **48**(15): p. 6.
28. Jia, F.D., et al., *Laser Scattering Diagnosis of a 60-Hz Non-Equilibrium Atmospheric Pressure Plasma Jet*. Applied Physics Express, 2011. **4**(2): p. 3.
29. Penney, C.M., R.L. Stpeters, and M. Lapp, *ABSOLUTE ROTATIONAL RAMAN CROSS-SECTIONS FOR N₂, O₂, AND CO₂*. Journal of the Optical Society of America, 1974. **64**(5): p. 712-716.
30. Penney, C., R.S. Peters, and M. Lapp, *Absolute rotational Raman cross sections for N₂, O₂, and CO₂*. JOSA, 1974. **64**(5): p. 712-716.
31. Long, D.A. and D. Long, *Raman spectroscopy*. Vol. 206. 1977: McGraw-Hill New York.
32. Hoskins, L.C., *Pure rotational Raman spectroscopy of diatomic molecules*. Journal of Chemical Education, 1975. **52**(9): p. 568.
33. Eckbreth, A.C., *Laser diagnostics for combustion temperature and species*. Vol. 3. 1996: CRC Press.
34. Klarenaar, B.L.M., et al., *Note: Rotational Raman scattering on CO₂ plasma using a volume Bragg grating as a notch filter*. Review of Scientific Instruments, 2015. **86**(4): p. 3.
35. Deng, X., et al., *Absolute and relative emission spectroscopy study of 3 cm wide planar radio frequency atmospheric pressure bio-plasma source*. Applied Physics Letters, 2015. **107**(5): p. 053702.
36. Hofmann, S., et al., *Power dissipation, gas temperatures and electron densities of cold atmospheric pressure helium and argon RF plasma jets*. Plasma Sources Science and Technology, 2011. **20**(6): p. 065010.
37. Lieberman, M.A. and A.J. Lichtenberg, *Principles of plasma discharges and materials processing*. 2005: John Wiley & Sons.
38. Winchester, M.R. and R. Payling, *Radio-frequency glow discharge spectrometry: A critical review*. Spectrochimica Acta Part B-Atomic Spectroscopy, 2004. **59**(5): p. 607-666.
39. Nilsson, J.W. and S.A. Riedel, *Introductory circuits for electrical and computer engineering*. 2001: Pearson Education.
40. Yanguas-Gil, A., et al., *Optical and electrical characterization of an atmospheric pressure microplasma jet for Ar/CH₄ and Ar/C₂H₂ mixtures*. Journal of applied physics, 2007. **101**(10): p. 103307.
41. Reuter, S., *Formation mechanisms of atomic oxygen in an atmospheric pressure plasma jet characterised by spectroscopic methods*. 2008: Cuvillier Verlag.
42. Cullen, P.J. and V. Milosavljević, *Spectroscopic characterization of a radio-frequency argon plasma jet discharge in ambient air*. Progress of Theoretical and Experimental Physics, 2015(6): p. 17.
43. Kawamura, E., et al., *Particle-in-cell and global simulations of α to γ transition in atmospheric pressure Penning-dominated capacitive discharges*. Plasma Sources Sci. Technol, 2014. **23**(035014): p. 0963-0252.
44. Wang, L., et al., *Mechanisms of sustaining a radio-frequency atmospheric pressure planar discharge*. Plasma Sources Science and Technology, 2017. **26**(7): p. 075012.
45. Fridman, A., *Plasma chemistry*. 2008: Cambridge university press.
46. Mitchner, M. and C. Kruger, *Partially Ionized Gasses*. Wiley&Sons. New York, 1973.
47. Nikiforov, A.Y., et al., *Characterization of a planar 8 mm atmospheric pressure wide radiofrequency plasma source by spectroscopy techniques*. Plasma Physics and Controlled Fusion, 2015. **58**(1): p. 014013.
48. Raizer, Y.P., *Gas discharge physics*. 1991.
49. Vorac, J., *massiveOES*. Atlassian Inc.,[Online]. Available: https://bitbucket.org/OES_muni/massiveoes. [Accessed 26 11 2018].
50. Bruggeman, P., et al., *Electronic quenching of OH(A) by water in atmospheric pressure plasmas and its influence on the gas temperature determination by OH(A-X) emission*. Plasma Sources Science & Technology, 2010. **19**(1): p. 7.